CSIRO PUBLISHING

Australian Journal of Physics

Volume 51, 1998
© CSIRO 1998

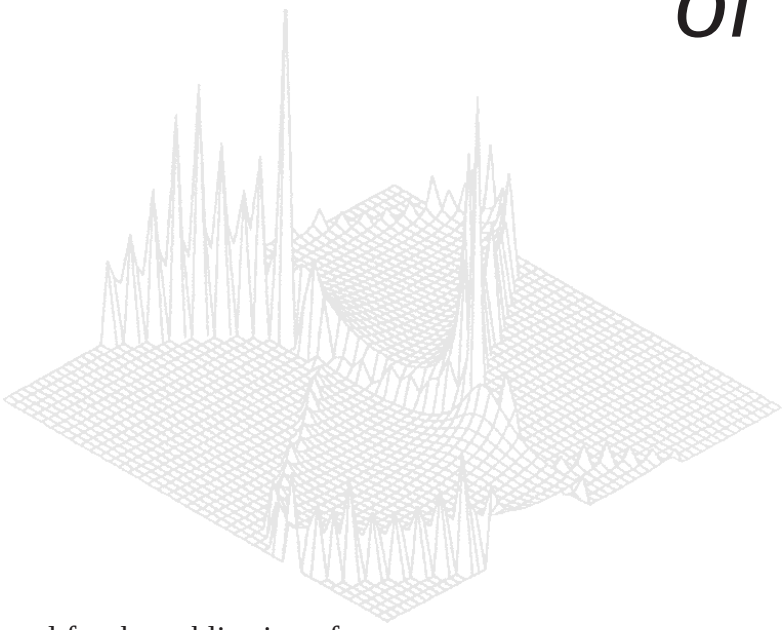

A journal for the publication of
original research in all branches of physics

www.publish.csiro.au/journals/ajp

All enquiries and manuscripts should be directed to
Australian Journal of Physics
CSIRO PUBLISHING
PO Box 1139 (150 Oxford St)
Collingwood Telephone: 61 3 9662 7626
Vic. 3066 Facsimile: 61 3 9662 7611
Australia Email: peter.robertson@publish.csiro.au

Published by **CSIRO** PUBLISHING
for CSIRO and the
Australian Academy of Science

Aust. J. Phys., 1998, **51**, 183–200

Hyperfine Magnetic Fields for Os, Ir and Pt in Iron: Pre-equilibrium Effects, Domain Rotation and the Aharoni Effect*

A. E. Stuchbery and E. Bezakova

Department of Nuclear Physics, Research School of Physical Sciences and Engineering, Australian National University, Canberra, ACT 0200, Australia.

Abstract

Hyperfine fields acting on subnanosecond excited states of impurity nuclei recoil-implanted into ferromagnetic hosts are being studied. These measurements are sensitive to effects on the picosecond time-scale that accompany implantation as well as to phenomena of longer duration. We review our recent work, mainly on 5d impurities implanted into iron, which has concerned: (i) the behaviour of the transient field at low recoil velocities, (ii) the dependence (magnitude and direction) of the hyperfine field on the applied field, (iii) the site distribution of the implanted nuclei, and (iv) the time the static field takes to reach equilibrium after implantation. It is found that the static hyperfine field takes about 10 ps after implantation to reach equilibrium. Once equilibrium is established the internal fields may be misaligned with respect to the direction of the external field, but this is associated with domain rotation in an incompletely saturated sample rather than with the 'Aharoni effect'.

1. Introduction

Magnetic moment systematics of low-lying collective nuclear states are largely confined to stable nuclei. Our goal over the next few years is to extend the g-factor systematics for low-excitation states in heavy nuclei to include neutron-deficient nuclei. These measurements present many experimental challenges, largely because the states of interest have subnanosecond lifetimes, which means that a measureable precession can be obtained only by employing the integral perturbed angular correlation technique in conjunction with intense hyperfine magnetic fields present at impurity nuclei implanted into ferromagnetic hosts.

Along with several technical problems (see e.g. Stuchbery *et al.* 1996*b*), there are several potential problems inherent in the implantation perturbed angular correlation (IMPAC) technique. Matters that must be considered include:

(i) corrections for the transient field effect;
(ii) whether the hyperfine field is parallel (or antiparallel) to the applied field;
(iii) whether the implanted nuclei all experience the same magnetic interaction; and
(iv) the time the static field takes to reach equilibrium after implantation.

* Refereed paper based on a contribution to the International Workshop on Nuclear Methods in Magnetism, held in Canberra on 21–23 July 1997.

© CSIRO Australia 1998 10.1071/PH97059 0004-9506/98/020183$10.00

It is these matters, which in time-integral measurements cannot always be treated independently, that are the focus of the present work.

The present paper is set out as follows: A short account of the experimental procedures and analysis techniques is presented first. Our studies of transient fields at low velocities, which have implications for the other measurements reported below, are discussed in Section 3. We then present and discuss the results of our studies of the dependence of the internal fields, both static and transient, on the magnitude of the external polarising field. These measurements concern the conditions under which the internal fields can be assumed to be parallel to the external field and as a by-product have implications for the site distribution of the implanted impurities. Finally, we present an update on measurements of static fields for iridium and neighbouring ions implanted into iron, for which the static hyperfine field appears to take about 10 ps after implantation to reach equilibrium.

The objective here is to present an overview of our most recent work which will be reported in detail elsewhere when completed. In the process of investigating the hyperfine fields, we have often found it necessary to measure precisely the nuclear properties (lifetimes and g-factors) of the probe states. Although this has been a time-consuming aspect of our work, it will not be discussed here.

2. Experimental Procedures and Analysis

The measurements reported here are largely 'standard' IMPAC measurements, performed using Coulomb excitation of stable target nuclei, similar to measurements described previously (e.g. Anderssen and Stuchbery 1995; Stuchbery *et al.* 1996*a*, and references therein). A heavy ion beam is employed to Coulomb-excite and recoil-implant target nuclei into an iron foil placed behind the target material, as illustrated in Fig. 1. The beam species, beam energy and thickness of the Fe layer are chosen to either ensure that the recoiling target nuclei all stop in the Fe layer (static field measurement) or all fully traverse the Fe layer and stop

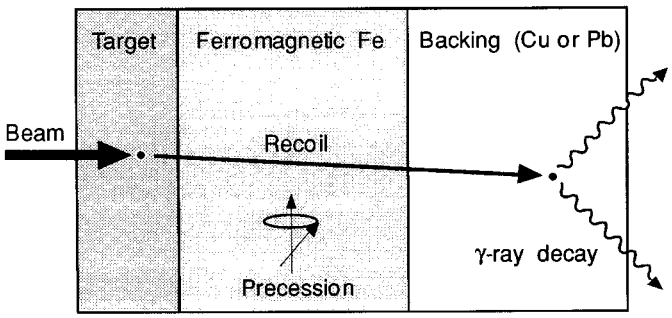

Fig. 1. Schematic representation of the three-layer targets employed in 'thin foil' transient field measurements. Nuclear states of interest are Coulomb excited and recoil implanted by a heavy-ion beam. The thickness of the ferromagnetic layer is chosen to ensure that all of the recoiling nuclei traverse it and stop in the non-magnetic backing layer. For static field measurements, either the energy of the recoils is reduced, or the thickness of the ferromagnetic layer is increased so that all of the recoiling nuclei stop in that layer.

in the nonmagnetic backing (transient field measurement). Backscattered beam ions are detected in coincidence with γ rays de-exciting the implanted nuclei (see Fig. 2).

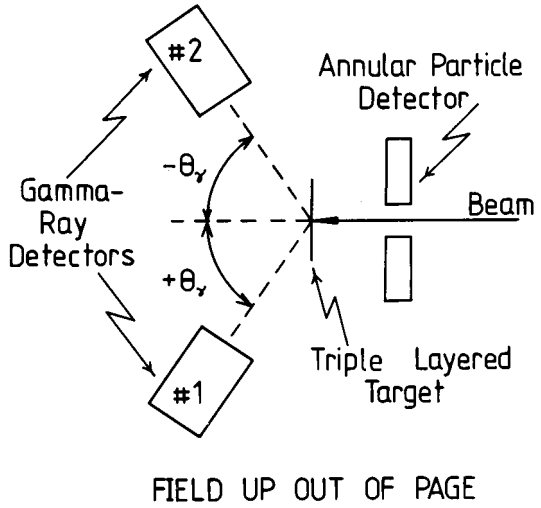

Fig. 2. Simplified plan of the experimental apparatus. Gamma-rays de-exciting the nuclear states of interest are detected in coincidence with backscattered beam particles. In most measurements a second pair of γ-ray detectors is placed in the backward quadrant.

In the general case of an energetic ion slowing to rest in a polarised ferromagnet, the nucleus will experience the transient hyperfine field $B_{\rm tr}(v[t])$ while the ion is in motion, and the static hyperfine field $B_{\rm st}$ after it comes to rest. The transient field is always in the same direction as the external field $B_{\rm ext}$, whereas the static field can be in the opposite direction.

The precession of the nucleus (typically between $\sim 0{\cdot}05$ and ~ 1 radian) is determined from the integral perturbed particle-γ angular correlation

$$W(\vartheta_\gamma, \pm B_{\rm ext}) = \sum_{k=0,2,4} (b_k / \sqrt{1 + (k\omega\tau)^2}) \cos[k(\vartheta_\gamma \mp \Delta\theta_k \mp \Delta\theta_{\rm tr})] \,, \qquad (1)$$

where ϑ_γ is the angle of γ-ray detection with respect to the beam axis,

$$\omega\tau = -g \frac{\mu_N}{\hbar} B_{\rm st} \tau \,, \qquad (2)$$

$$\tan(k\Delta\theta_k) = k\omega\tau \,, \qquad (3)$$

g is the g-factor and τ is the lifetime of the state of interest. The angular distribution coefficients b_k can be calculated from the theory of Coulomb excitation. As the transient field precession $\Delta\theta_{\rm tr}$ is small and acts for a time that is short

compared with the lifetime of the state, its influence on the angular correlation is treated as a pure rotation through an angle

$$\Delta\theta_{\rm tr} = -g\,\frac{\mu_N}{\hbar}\int_{T_1}^{T_2} B_{\rm tr}(v[t])\,e^{-t/\tau}\,dt\,, \tag{4}$$

where $T_{1(2)}$ is the entrance (exit or stopping) time for the ions traversing the ferromagnetic foil. The transient field effect can be important whether the static field precession $\omega\tau$ is large or small (see e.g. Fig. 4 of Stuchbery *et al.* 1996*a* and the discussion therein).

If the internal field is misaligned with respect to the external field, equation (1) must be modified. Assuming the internal field is equally distributed on a cone at angle β to the external field, the angular correlation becomes (Ben-Zvi *et al.* 1967)

$$W(\vartheta_\gamma,\beta,B) = 4\pi\sum_{k,N,P}\frac{a_k}{2k+1}|Y_k^N(\tfrac{\pi}{2},0)|^2\frac{\cos(N\vartheta_\gamma - P(\Delta\theta_P+\Delta\theta_{\rm tr}))}{\sqrt{1+(P_{\omega\tau})^2}}$$

$$\times\,[d^k_{PN}(\beta)]^2\,, \tag{5}$$

where $\tan(P\Delta\theta_P) = P\omega\tau$, Y_k^N is a spherical harmonic and d^k_{PN} is the matrix for the second Euler rotation (about the y axis). The coefficients a_k and the b_k coefficients mentioned above are linear combinations of each other.

A schematic of the experimental apparatus is shown in Fig. 2. At least one pair of γ-ray detectors was employed, as shown in Fig. 2, but in most measurements an additional pair of detectors was placed in the backward quadrant at $\pm115^\circ$ to the beam. The forward detectors were usually placed at complementary angles ($\vartheta_2 = -\vartheta_1$) with respect to the beam axis. The magnetic field direction, perpendicular to the plane of the γ-ray detectors, was reversed in direction frequently during the measurements.

It is sometimes helpful to eliminate normalisation and efficiency factors by analysing the data in terms of double ratios ρ and asymmetries ϵ:

$$\rho(\vartheta_1,\vartheta_2) = \sqrt{\frac{W(\vartheta_1,\uparrow)\;W(\vartheta_2,\downarrow)}{W(\vartheta_1,\downarrow)\;W(\vartheta_2,\uparrow)}}\,, \tag{6}$$

where the arrows indicate the direction of the external field and

$$\epsilon(\vartheta_1,\vartheta_2) = \frac{1-\rho(\vartheta_1,\vartheta_2)}{1+\rho(\vartheta_1,\vartheta_2)}\,. \tag{7}$$

In the case where $\vartheta_1 = -\vartheta_2 = \vartheta_\gamma$, $\epsilon(\vartheta_\gamma,-\vartheta_\gamma)$ is formally equivalent to

$$\epsilon(\vartheta_\gamma,-\vartheta_\gamma) \equiv \frac{W(\vartheta_\gamma,\downarrow) - W(\vartheta_\gamma,\uparrow)}{W(\vartheta_\gamma,\downarrow) + W(\vartheta_\gamma,\uparrow)}\,. \tag{8}$$

If the total precession angle is small ($\lesssim 150$ mrad) we can define

$$\Delta\theta = \omega\tau + \Delta\theta_{\rm tr}\,. \tag{9}$$

Then we have

$$\Delta\theta = \frac{\epsilon}{S}\,, \tag{10}$$

where S is the logarithmic derivative of the angular correlation at the detector angle ϑ_γ.

3. Transient Fields at Low-velocity Tl Ions in Fe

It was discovered about 30 years ago that nuclei implanted into a ferromagnetic host with velocities of the order of a few per cent of the speed of light experience an intense hyperfine magnetic field (Borchers *et al.* 1968). While these authors suggested immediately that the transient field (TF) might arise from the *capture* of polarised electrons by the moving ion (PEC), Lindhard and Winther (LW) (1971) soon proposed a model in which the field is produced by the *scattering* of polarised electrons. In the electron capture model the TF increases with ion velocity, whereas the field decreases with increasing velocity in the LW theory:

$$B_{\rm LW} = \frac{16\pi^2}{3}\mu_{\rm B}N_{\rm P}Z\left[1+\left(\frac{Z}{84}\right)^{2.5}\right]\frac{v_0}{v_r}\,; \tag{11}$$

$$v_r = v \text{ for } v > v_p \sim 0{\cdot}78v_0; \quad v_r = v_p \text{ for } v < v_p \sim 0{\cdot}78v_0.$$

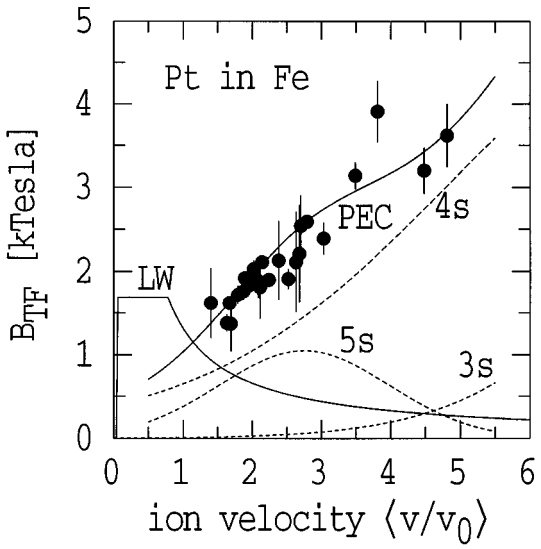

Fig. 3. Transient field strengths as a function of velocity for Pt ions in iron, showing the prediction of the Lindhard–Winther (LW) model and a semi-empirical fit based on the polarised electron capture (PEC) model. In all measurements the TF is sampled over a range of ion velocities. The data points are plotted at the average velocity. See Stuchbery *et al.* (1994) for further details.

Here $\mu_B N_P = 0{\cdot}175$ T for Fe and $v_0 = c/137$ is the Bohr velocity. The LW field is usually assumed to cut off at very low velocities, corresponding to ion energies of a few keV. (The exact value is not critical.) Fig. 3, adapted from Stuchbery *et al.* (1994), compares measured transient fields for Pt in Fe with the LW and PEC models.

Despite experimental observations that the TF increases with ion velocity, it has proved difficult to measure the TF strength at low ion velocities where the LW effect would be dominant, if present at all. The ideal probe state should be in a high-Z nucleus, and have a large g-factor and short lifetime. If possible, the probe element should have a small static hyperfine field. The lowest $\frac{5}{2}^+$ states in ^{203,205}Tl, with $g \sim 0{\cdot}8$ and $\tau \sim 1{\cdot}5$ ps, fit these requirements. (Before the hyperfine fields could be studied, more precise g-factor measurements were required; these will be reported elsewhere.)

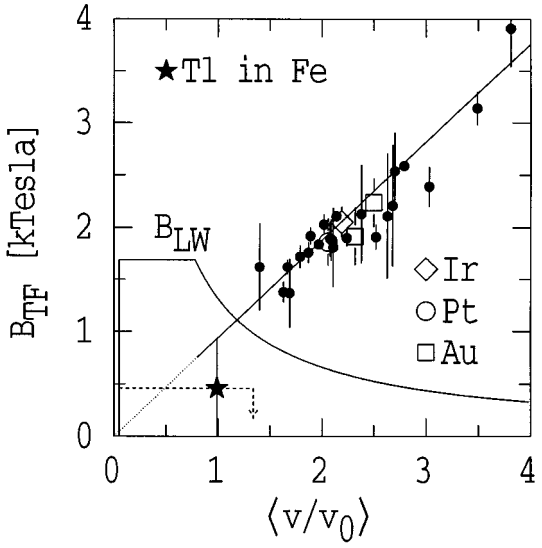

Fig. 4. Transient field strengths as a function of velocity for Ir, Pt, Au and Tl ions in iron (cf. Fig. 3). The point for Pt designated by the larger open circle was measured simultaneously with the Ir datum. The best fit to an assumed linear velocity dependence is shown. The solid portion of the straight line indicates the velocity range sampled by the 'thin foil' measurements on Ir, Pt and Au. The 'thick foil' measurement on Tl described in the text samples the TF over the velocity range indicated by the dashed line (and arrow).

The magnitude of the TF acting on low-velocity Tl ions recoil-implanted into a $7{\cdot}5$ μm thick Fe foil following Coulomb excitation with 40 MeV ^{16}O beams was measured using the $\frac{5}{2}^+$ states in ^{203,205}Tl as probes. The result is plotted in Fig. 4 along with TF data for Pt and neighbouring ions in Fe at higher recoil velocities ($> 0{\cdot}8v_0$). At low velocities the TF is smaller than that predicted by the LW theory and remains consistent with the empirical, velocity-proportional parametrisation, and hence with the polarised-electron-capture model.

In agreement with earlier work employing lighter probes (de Raedt *et al.* 1980; Eberhardt and Dybdal 1980), we find no evidence for a transient field of the

magnitude proposed by Lindhard and Winther. As there is no empirical evidence for a TF due to electron scattering at low ion velocities, and as the LW theory has also been criticised on theoretical grounds (see Anderssen and Stuchbery 1995 for references and further discussion), we proceed on the assumption that it does not exist. An extrapolation of the empirical velocity-dependence of the TF to zero velocity will be sufficiently accurate for most applications, including those in the following sections.

4. Misaligned Hyperfine Fields

The first evidence that the internal hyperfine field may not be parallel to the external applied field, even in the case where the macroscopic sample is apparently saturated, was presented by Ben-Zvi *et al.* (1967). They showed, from IMPAC measurements on ^{186}W and ^{148}Nd implanted into Ni and Fe hosts, that the direction of the internal field could be misaligned with the external field direction by angles of about 20° to 30° for magnetising fields of about 0·1 T. (This was the field on the pole tip—the field measured at the centre of the target with the foil removed was about 0·04 T; see footnote 4 of Aharoni 1969.) The internal field direction was apparently equally distributed on a cone about the external field direction. Krane and co-workers (1973, 1974) subsequently examined the low temperature orientation of several transition metal impurities in Fe, finding that complete orientation of the local field required external fields far in excess of those needed for saturation.

To explain the locally misaligned hyperfine fields, Aharoni (1969, 1970*a*, 1970*b*) proposed a microscopic mechanism associated with magnetostriction forces on oversize impurities in the host matrix. Further theoretical investigations were performed by Muggli (1973) and Andriessen and Postma (1983). Unfortunately the theory contains many approximations and lacks predictive power.

Many workers avoid the 'Aharoni' or 'cone' effect by using very large external fields, but this is not always an attractive option. In our work, a compromise value of the applied field must be found that is strong enough to saturate the host and yet, at the same time, is so weak that it causes a negligible deflection of the incident beam ions. (Beam bending mimics the precession of the nucleus.)

There have been several measurements following up on the nuclear orientation measurements of Krane *et al.* To our knowledge a clear difference was observed between the relative magnetisation deduced from γ-ray anisotropy and the bulk magnetisation in only one subsequent nuclear orientation measurement, where ^{60}Co was diffused into an iron plate 0·3 mm thick (Kieser *et al.* 1974). In contrast, Stewart *et al.* (1977) found that magnetic saturation accompanied the alignment of the quantisation axis for cobalt in iron foils 1 to 2·5 μm thick. They suggested that the effect observed by Krane *et al.* may have been due to a proportion of the diffused nuclei experiencing a non-uniform region of magnetisation at the edge of the 0·1 mm thick foil. Surface magnetisation measurements by de Waard *et al.* (1975) and the observation of γ anisotropies independent of applied fields between 0·0475 and 0·114 T for ^{60}Co in thin (25·4 μm) Fe foils (Barr and Sapp 1977) support this conclusion. Furthermore, Visser *et al.* (1984) found that the field at ^{131}I in Fe follows the field in the domain and van Walle *et al.* (1986) showed that there was no need to invoke 'misaligned' internal fields for Au implanted into Fe if the samples were prepared well, again pointing out the

role of surface magnetisation. There is apparently no uncontroverted evidence in the literature for the 'Aharoni/cone' effect in nuclear orientation and NMR measurements.

Lindgren *et al.* (1976) used time differential γ-γ perturbed angular correlation techniques to study the hyperfine field for Cd in Ni as a function of magnetising field. No change in the hyperfine field was observed for external fields above $0{\cdot}07$ T.

Concerning in-beam IMPAC measurements like those of Ben-Zvi *et al.*, there have been few specific measurements of the static hyperfine field dependence on external field. Although several authors were concerned about the matter [e.g. Sioshanshi *et al.* (1972) and Garber *et al.* (1974)], to our knowledge, only Sie *et al.* (1971) reported measurements for Os in Fe with external fields between $0{\cdot}04$ and $0{\cdot}26$ T. No change in internal field was observed for external fields above about $0{\cdot}06$ T. As part of their study of Gd as a host for IMPAC measurements, Skaali *et al.* (1976) measured the combined static and transient field precession for ^{150}Sm in 25 μm thick Gd as a function of external field up to about $0{\cdot}45$ T. A reduction in the precession was observed only below $0{\cdot}1$ T. It should be noted that surface effects are less likely to be important in IMPAC measurements because the nuclei of interest are usually implanted to a depth of at least 1 μm.

After it was discovered in the mid 1970s that the transient field increases with ion velocity, attention shifted to transient-field (TF) IMPAC measurements. Goldberg *et al.* (1978) measured the transient field precessions of ^{16}O in 1 μm Fe, finding that the maximum precession was already attained with a magnetising field of $\sim 0{\cdot}003$ T. Ward *et al.* (1979) measured TF precessions for ^{169}Tm in $\sim 3{\cdot}8$ μm thick Fe for external fields between $0{\cdot}026$ and $0{\cdot}174$ T. The precession had saturated by $0{\cdot}07$ T.

The main evidence for misaligned hyperfine fields is therefore that presented in the original paper of Ben-Zvi *et al.* While their data could have a microscopic explanation in the Aharoni effect, or perhaps some other local phenomenon, similar effects in the perturbed angular correlations could also be produced by macroscopic domain rotation if the host were not fully saturated. Further investigation is required.

(4a) Measurements Performed

The static field dependence on external field was measured for ^{188,190,192}Os, ^{191,193}Ir and ^{194,196}Pt implanted into Fe, following Coulomb excitation with beams from the ANU 14UD Pelletron accelerator. A summary of the measurements performed is given in Table 1. Details of the targets appear in Table 2. Most of the targets had been used previously for studies of transient fields, static fields or for measuring g-factors (Anderssen and Stuchbery 1995; Stuchbery *et al.* 1992, 1994, 1996*a*). In all cases the Fe foils were rolled to the desired thickness, beginning with $99{\cdot}85\%$ pure foils, most frequently ~ 5 μm thick, obtained from Goodfellow Cambridge Limited. After rolling, the foils were annealed in vacuum for 20 min, at about 800°C. They were then allowed to cool slowly to room temperature. The magnetisations of the Fe foils were measured with the Rutgers Magnetometer (Piqué *et al.* 1989) after the in-beam studies.

Table 1. Summary of measurements

Run	Target[A]	Beam	Measurement[B]	ϑ_F[C] (°)	ϑ_B[C] (°)	B_{ext} (T)
I	^{188,190,192}Os	36 MeV ^{16}O	SF vs B_{ext}	± 65	—	0·017–0·53
			AC	±(30–65)	—	0·24
II	^{nat}Pt	36 MeV ^{16}O	SF vs B_{ext}	± 65	—	0·017–0·53
			AC	±(0–65)	—	0·05, 0·53
III	^{198}Pt+^{191,193}Ir	36 MeV ^{16}O	SF vs B_{ext}	± 30	—	0·05–0·53
			AC	±(0–65)	—	0·05, 0·53
IV	^{nat}Pt	36 MeV ^{16}O	BB vs B_{ext}	± 65	—	0·05–0·53
			AC	±(0–65)	—-	0·24
V	^{188,190,192}Os	36 MeV ^{16}O	SF vs B_{ext}	±(30, 65)	±115	0·017, 0·044, 0·08
			AC	±(0–65)	±115	0·017, 0·08
VI	^{nat}Pt	36 MeV ^{16}O	SF vs B_{ext}	±65	±115	0·017, 0·044, 0·08
			AC	±(0–65)	±115	0·017
VII	^{188}Os +^{196}Pt	36 MeV ^{16}O	SF vs B_{ext}	±(30, 65)	±115	0·017, 0·044, 0·08
VIII	^{188,190,192}Os	150 MeV ^{58}Ni	TF vs B_{ext}	±65	±115	0·017, 0·044, 0·08
			AC	±(0–65)	±115	0·044
IX	^{188}Os+^{196}Pt	80 MeV ^{32}S	TF vs B_{ext}	±65	±115	0·017, 0·044, 0·08

[A] See Table 2 for details of targets.
[B] SF (TF): static (transient) hyperfine field; BB: beam bending; AC: angular correlation.
[C] γ-ray detector angles to the beam axis in the forward (F) and backward (B) quadrants.

Table 2. Details of targets

Target	Composition[A] I	Composition[A] II	Thickness (mg/cm^2) I	Thickness (mg/cm^2) II	Thickness (mg/cm^2) Fe[B]	Backing	Runs		
1	^{188,190,192}Os[C]		0·9		3·3	Pb	I	V	VIII
2	^{nat}Pt		0·44		4·3		II	VI	
3	^{198}Pt	^{nat}Ir	0·15	0·89	1·63	Cu	III		
4	^{nat}Pt		0·42		Cu	IV			
5	^{196}Pt	^{188}Os	0·44	0·38	1·53	Pb	VII	IX	

[A] Composition of the 'target' layers in the order encountered by the beam. Layers of osmium were electroplated; iridium and platinum were sputtered.
[B] Iron layer in which the excited 'target' ions experience the hyperfine fields.
[C] Natural Os laced with extra ^{188}Os. See Stuchbery *et al.* (1992) for further details.

Initially, a survey was performed employing a relatively large electromagnet that produced fields up to about 0·5 T at the target location (Runs I–III). The stray fields produced were quite pronounced at the highest settings so it proved necessary to measure the beam bending for this apparatus (Run IV). Following the survey, more detailed measurements were made in the lower field regime (0·017 and 0·08 T) with a more compact target chamber and electromagnet (Runs V–VII). Less extensive measurements were performed for $B_{ext} = 0·044$ T since this had been studied previously (Stuchbery 1996*a*). The transient field dependence on external field was then measured for two of the targets (Runs VIII–IX). The applied fields we quote were measured at the position of the beam spot at the centre of the target location, but with the target removed. (Nominal

applied fields of 0·05 T reported in papers from our group over the past decade correspond to 0·044 T by this reckoning.)

(4b) Results and Analysis

For the initial survey, the *apparent* static field strengths were deduced as a function of the external, polarising field from observations of ϵ at $\vartheta_\gamma = \pm 65°$. Results are displayed in Fig. 5. Appropriate corrections were made for beam bending and the transient-field effect, hence the saturation values of the apparent fields can be interpreted quantitatively, but the apparent fields should be interpreted only qualitatively once the field drops below its saturation value. The results for Os and Ir shown in Fig. 5 are reminiscent of the nuclear orientation results obtained by Krane *et al.* (1973). In contrast, Pt seems to show no effect—this turns out to be an artefact originating from the fact that the precessions for the Pt isotopes are less than 100 mrad (see below).

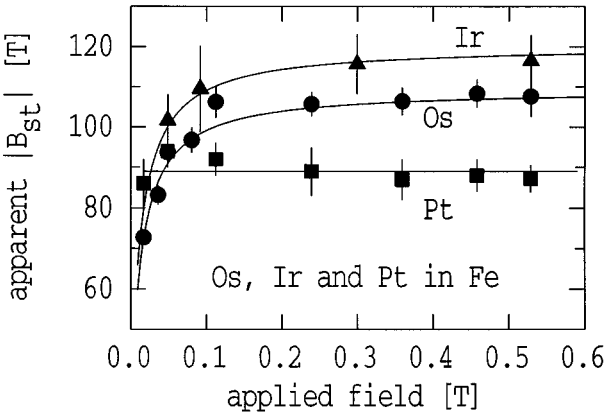

Fig. 5. *Apparent* static hyperfine field as a function of external field for ^{188,190,192}Os, ^{191,193}Ir and ^{194,196}Pt ions recoil-implanted into iron. These apparent field strengths should not be interpreted quantitatively at low external fields. The lines are drawn to guide the eye. As discussed in the text, the seeming difference in behaviour for Pt is not fundamental but arises from the fact that the nuclear lifetimes, and hence the observed precessions, are small in that case.

The perturbed angular correlations measured in the low-field regime were analysed assuming the internal field direction lies isotropically on a cone at angle β to the applied field direction and the parameters β and $\omega\tau$ were varied to obtain the best fit. This procedure should be viewed as a parametrisation of the real situation because some texture effects are expected below full saturation of the host, in which case, the hyperfine fields would not be equally distributed around the cone. The angular correlations and the $\epsilon(\vartheta_1, \vartheta_2)$ values derived from them were examined. We also explored the implications of assuming some fraction of the implanted nuclei reside on low-field sites.

Results of fits to $\epsilon(\vartheta_1, \vartheta_2)$ for ^{192}Os with external fields of 0·017 T and 0·08 T are shown in Fig. 6. At 0·08 T the Os isotopes experience essentially the full hyperfine field (97±3%) parallel to the external field. For $B_{\rm ext} = 0{\cdot}017$ T

the hyperfine field is both misaligned ($\beta \approx 26{\cdot}5°$) and apparently reduced in magnitude (89±3%). The dotted curve in the figure shows the best fit to the $B_{\text{ext}} = 0{\cdot}017$ T data with $\beta = 0$. It is clear that the hyperfine field becomes misaligned with respect to the external field at the lower values of the external field. It is also evident that the implanted nuclei must reside predominantly on unique sites as the presence of more than a few per cent of the nuclei on low-field sites is inconsistent with the observed perturbed angular distributions.

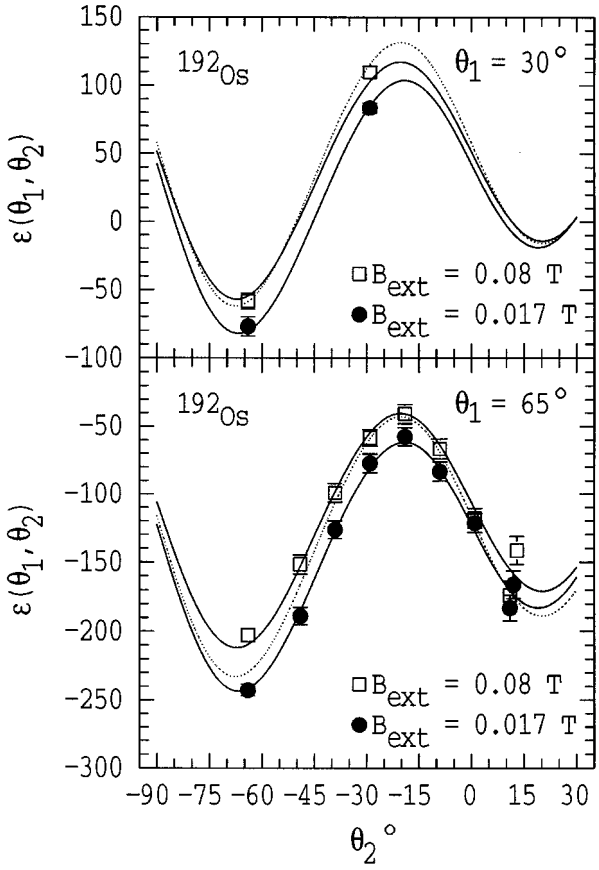

Fig. 6. Fits to the generalised asymmetry parameter $\epsilon(\vartheta_1, \vartheta_2)$ [equation (7)] for ^{192}Os implanted into iron where the external field is $0{\cdot}017$ T and $0{\cdot}08$ T. Here ϑ_1 is either 30° (upper panel) or 65° (lower panel) while ϑ_2 varies between −65° and +15°. Note that $\epsilon(\vartheta_1, \vartheta_2)$ is an absolute quantity; there are no normalisation factors in the fits. At $B_{\text{ext}} = 0{\cdot}08$ T the internal and external fields are aligned, but at $B_{\text{ext}} = 0{\cdot}017$ T the best fit is obtained if the internal field has a cone angle of $26{\cdot}5°$ with respect to the external field. The dotted curve shows the best possible fit to the data for $0{\cdot}017$ T assuming the internal and external fields are aligned.

As mentioned above, the Pt isotopes are relatively insensitive to the misalignment of the hyperfine field because the precessions are small (due to shorter lifetimes). For the same reason, it is impossible to obtain direct evidence for misaligned

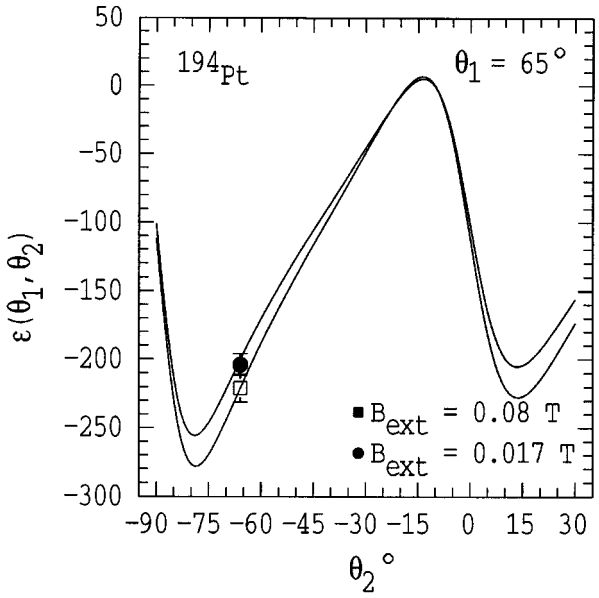

Fig. 7. Similar to Fig. 6, but for ^{194}Pt. As the precessions are smaller than for the Os isotopes, it is possible only to measure an effective internal field strength which gives no information about its direction. The solid curves show (i) the fit to the datum for $B_{\rm ext} = 0{\cdot}08$ T assuming the internal field is parallel to the external field and (ii) the predicted behaviour of $\epsilon(\vartheta_1, \vartheta_2)$ at $B_{\rm ext} = 0{\cdot}017$ T, scaled from (i) assuming that the internal field for Pt becomes misaligned like that found for Os.

fields from the Pt measurements alone. Nevertheless, as Fig. 7 shows, the data for the platinum isotopes are consistent with the same misalignment angles and reductions in the local field strength as derived from the osmium data.

Transient field strengths measured as a function of applied field for two of the targets are shown in Fig. 8. The transient field precessions are compared with the measured magnetisation for the osmium target in Fig. 9. As is usually expected (Shu *et al.* 1980), the transient field precessions scale with the relative magnetisation of the sample. The reduced TF precessions observed at lower fields can be explained within the precision of the data by the same mechanisms as in the static field case, i.e. for $B_{\rm ext} = 0{\cdot}017$ T the reduced TF can be explained by an effective field that is both misaligned ($\beta \approx 26{\cdot}5°$) and reduced in magnitude ($\approx 90\%$). The solid curves in Figs 8 and 9, drawn to guide the eye, parametrise the bulk magnetisation as (Bozorth 1951)

$$M = M_S(1 - C/B_{\rm ext})\,, \tag{12}$$

where the parameter C was varied to fit the data. The dashed curve in Fig. 9 shows the expected behaviour (Bozorth 1951; Aharoni 1969) for polycrystalline Fe foils near saturation

$$M = M_S[1 - cK^2/(M_S B_{\rm ext})^2]\,, \tag{13}$$

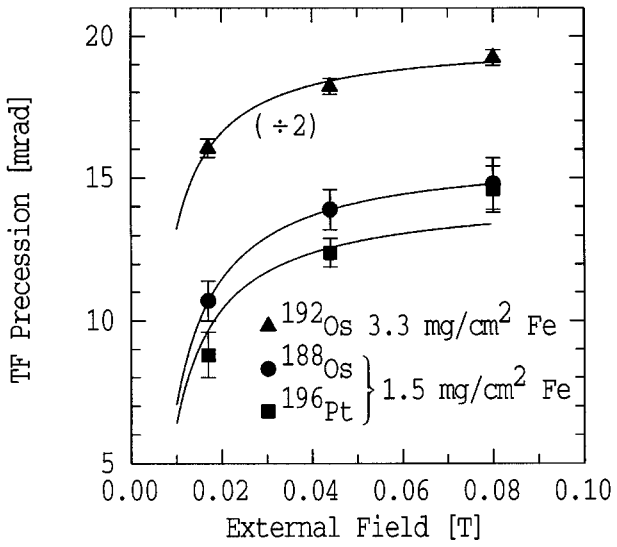

Fig. 8. Transient field precessions as a function of the external field for the designated isotopes of Os and Pt in thin iron foils. The precessions for ^{188}Os and ^{196}Pt were measured simultaneously as they traversed the same foil (Target 5 in Table 2). For presentation, the precessions of ^{192}Os traversing the thicker foil have been divided by two. The reduced precessions at lower external fields can be explained by the mechanisms deduced from the static field measurements (Fig. 6). As the ions experience the transient field while they traverse the foil, this suggests that the misaligned fields are due to domain rotation in a less than fully saturated sample, rather than to a local effect such as that proposed by Aharoni.

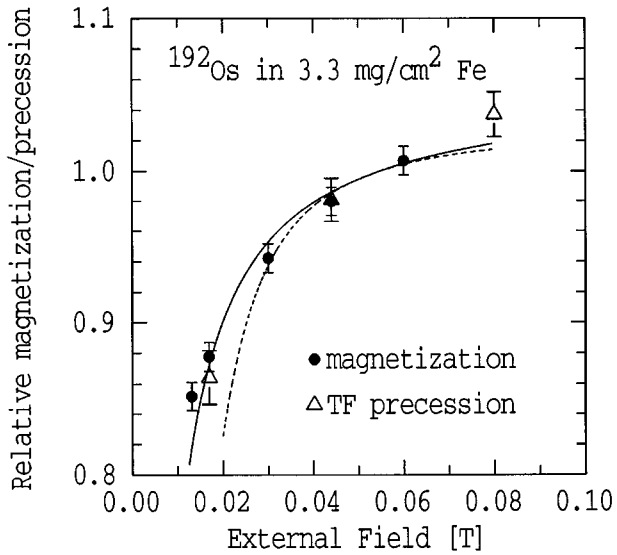

Fig. 9. Comparison of relative transient-field precessions and relative foil magnetisations for Target 1 (see Table 2). The TF data for ^{192}Os are the same as in Fig. 8. The solid curve is a fit to the magnetisation data assuming it varies with external field as specified by equation (12). The dashed curve shows the expected variation of the magnetisation near saturation [equation (13)].

where $c(K/M_S)^2 = 7{\cdot}84 \times 10^{-5}$ [T^2]. For external fields above $0{\cdot}03$ T this expression describes the measured magnetisation of the foil very well.

Since the TF acts on ions in motion *through* the Fe foil (several microns thick), the observed effects must have a macroscopic origin. They are consistent with less than complete saturation of the foils below about $0{\cdot}08$ T. There is no evidence for microscopic misalignment of the internal field as in the Aharoni effect.

One unexpected result of the fits to the low-field data is that the misalignment angle seems to be quite sharply defined (the quality of the fits deteriorates if β departs by more than a few degrees from the angle of best fit). This seems unphysical. Metallurgical studies (see e.g. Barrett and Massalski 1966) indicate that the microcrystals in rolled and annealed iron foils prefer to align like cubes on their points in the plane of the foil. The (111) planes are in the plane of the foil with the [$\bar{2}$11] direction along the rolling direction. In the measurements, the [111] direction perpendicular to the plane of the foil would be along the beam direction and the the easy direction [100] would tend to be tilted at $35{\cdot}3°$ to the external field toward, or away from, the beam direction. We are investigating the implications of the assumption that the internal field is evenly distributed on a cone around the external field direction, which is dubious if the foil has texture.

From a practical perspective, the polycrystalline foils we use can be assumed to be saturated, and the external and internal fields can be assumed to be in the same direction, for external fields of $0{\cdot}08$ T.

Table 3. Comparison of hyperfine fields from IMPAC and NMR

Isotope	τ (ps)[A]	B_{IMPAC} (T)[B]	$B_{\max}$ (T)[C]	$B_{\mathrm{IMPAC}}/B_{\max}$
^{192}Os	414	109±1	109	1·00±0·01
^{193}Ir	100	119±1	142	0·84±0·01
^{194}Pt	60	89±2	123	0·72±0·02

[A] Lifetimes from Raman *et al.* (1987).
[B] IMPAC fields from the data presented in Fig. 5.
[C] Scaled to room temperature from values in the compilation of Krane (1983). Experimental errors are negligible compared with those on the IMPAC fields.

5. Pre-equilibrium Effects Following Implantation

A particularly interesting outcome of our recent work (Anderssen and Stuchbery 1995; Stuchbery 1996*a*) has been the observation that hyperfine fields for the 5d systems Os, Ir and Pt in iron appear to take about 10 ps to reach equilibrium following implantation. In Table 3 the saturation values of the hyperfine fields observed in the previous section are compared with the 'maximum' values found in NMR and radioactivity measurements. There is a correlation with the lifetime of the probe state. However, to study pre-equilibrium quenching of the static field it is best to perform precise, simultaneous measurements on nuclear states with different lifetimes in the same atomic species. This has proved to be difficult in the Os, Ir, Pt region. The first $\frac{5}{2}^+$ and $\frac{7}{2}^+$ states in ^{191}Ir and ^{193}Ir, with lifetimes between 29 and 127 ps, were chosen as suitable probe states. Their g-factors and lifetimes had to be measured accurately first (Bezakova *et al.* 1997).

After correction for the TF precession, the effective static field strength, B_{IMPAC}, can be extracted from the perturbed angular correlations. If we assume that the hyperfine field is zero for a time t_e after implantation, the observed effective field can be parametrised as

$$B_{\mathrm{IMPAC}} = (1 - f_0) \times B_{\max} \times e^{-t_e/\tau}\,, \tag{14}$$

where $B_{\max}$ is the field obtained in an NMR or radioactivity measurement with all of the nuclei on full-field sites. The factor $(1 - f_0)$ accounts for the fraction of nuclei that do not reside on full-field sites once equilibrium is established. Alternatively, if the hyperfine field comes to its equilibration value (from zero immediately after implantation) by a relaxation process with characteristic time τ_r, then the effective field is

$$B_{\mathrm{IMPAC}} = (1 - f_0) \times B_{\max} \times \left(\frac{\tau}{\tau_r + \tau}\right). \tag{15}$$

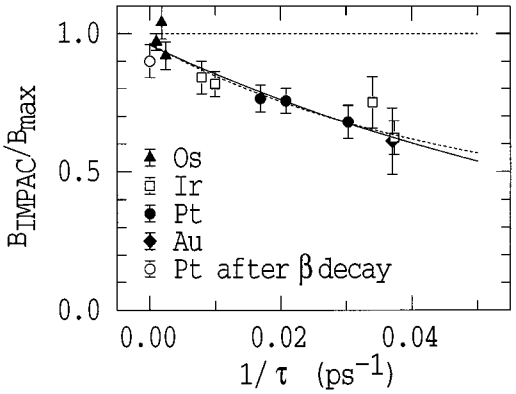

Fig. 10. Ratio of the static hyperfine fields measured by the IMPAC technique to the 'maximum' fields obtained from NMR measurements, plotted versus the inverse lifetime of the probe state used in the IMPAC measurement. The solid curve, a fit to equation (14), describes the situation where the hyperfine field is quenched altogether for a time $t_e = 11{\cdot}6$ ps after implantation, while the dashed curve, a fit to equation (15), assumes the hyperfine field 'relaxes' to its equilibrium value (from zero immediately after implantation) with a characteristic time $\tau_r = 14{\cdot}1$ ps.

As a convenient means of exposing pre-equilibrium effects, we may plot $B_{\mathrm{IMPAC}}/B_{\max}$ versus the inverse lifetime of the probe state $(1/\tau)$. The results for 5d impurities near iridium are displayed in Fig. 10. There is evidently a correlation between the lifetime of the probe state and the effective strength of the hyperfine field following implantation. Fits to equation (14) give $t_e = 11{\cdot}6 \pm 1{\cdot}4$ ps while fits to equation (15) yield $\tau_r = 14{\cdot}1 \pm 1{\cdot}9$ ps. In either case the hyperfine field takes of the order of 10 ps to reach equilibrium. Initially it was suggested (Anderssen and Stuchbery 1995; Stuchbery 1996*a*) that the static field

is quenched altogether for that time, perhaps due to the thermal spike. This was the simplest description of the data available at the time. Of course the equilibration time of the hyperfine field after implantation will be affected both by the timescale of the atomic rearrangements and by the equilibration time of the impurity-host spin system.

Alfter *et al.* (1997) have recently reported much longer equilibration times for erbium and dysprosium (4f) ions recoil-implanted into iron. This has led them to suggest that there is a relaxation of the hyperfine field following the thermal spike due to hindered antiferromagnetic coupling between 4f (and also 5d) impurity atoms and the iron host. In principle, this theory can be tested, and the different contributions to the equilibration process investigated, by making precise IMPAC measurements on several ion-host combinations. As the measurements are difficult, this would be a long-term project. Meanwhile, whatever the underlying mechanisms, these effects must be considered when using static fields to measure the g-factors of short-lived nuclear states immediately following ion implantation.

6. Summary and Conclusions

We have studied several aspects of the hyperfine fields which act upon heavy impurities recoil-implanted into iron hosts.

The transient field acting on low velocity ^{203}Tl and ^{205}Tl moving in iron was measured using the short-lived $\frac{5}{2}^{+}_{1}$ states as probes. No evidence was found for a transient field at low ion velocities ($v < v_0$) due to the scattering of polarised electrons. For practical purposes the empirical velocity dependence of the TF measured at higher velocities can be extrapolated to zero.

The external field dependence of the static hyperfine field acting on ^{188}Os, ^{190}Os, ^{192}Os, ^{191}Ir, ^{193}Ir, ^{194}Pt and ^{196}Pt implanted in polycrystalline iron was examined. While the internal field becomes increasingly misaligned with respect to the external field direction at fields below 0·08 T, this is associated with incomplete saturation of the foil (domain rotation), not with a microscopic effect like that proposed by Aharoni. The low field data are probably affected by the texture of the iron foils. This is being followed up. In our studies, the implanted osmium nuclei all experience the same magnetic interaction (within uncertainties of the order of a few per cent).

The static hyperfine field acting on 5d impurities implanted into iron takes of the order of 10 ps to reach equilibrium after implantation. The effect is associated with the implantation process and probably involves the quenching of the hyperfine field during the thermal spike, followed by a finite equilibration time for the spin system. Further measurements on a variety of impurity-host combinations are required to characterise and understand this phenomenon.

Acknowledgments

We would like to thank our colleagues T. R. McGoram, S. Bayer, M. P. Robinson, Dr T. Kibédi, Professor W. A. Seale, and Dr N. M. Thakur for assistance with the data collection. D. J. Pringle gave assistance with some of the measurements and data analysis whilst supported by a Summer Scholarship from the Department of Nuclear Physics, Australian National University. Professor H. H. Bolotin (University of Melbourne) collaborated on the work in Section 3. Susy Styles and Meera Parish participated in some of the measurements in Section 4

as part of the CSIRO Student Research Scheme. Professor N. Benczer-Koller (Rutgers University) made available the magnetometer and J. S. Holden (Rutgers) gave considerable assistance with the magnetisation measurements. Most of this work was carried out while one of us (AES) was supported by an Australian Research Council Senior Research Fellowship.

References

Aharoni, A. (1969). *Phys. Rev. Lett.* **22**, 856.
Aharoni, A. (1970*a*). *Phys. Rev.* B **2**, 3794.
Aharoni, A. (1970*b*). *Phys. Stat. Sol. (a)* **3**, 761.
Alfter, I., Bodenstedt, E., Knichel, W., Schüth, J., and Grawe, H. (1997). *Hyp. Interact.* **110**, 313.
Anderssen, S. S., and Stuchbery, A. E. (1995). *Hyp. Interact.* **96**, 1.
Andriessen, J., and Postma, H. (1983). *Hyp. Interact.* **15/16**, 305.
Barr, K. P., and Sapp, R. C. (1977). *Phys. Rev.* C **15**, 434.
Barrett, C. S., and Massalksi, T. B. (1966). 'Structure of Metals' (McGraw–Hill: New York).
Ben-Zvi, I., Gilad, P., Goldring, G., Hillman, P., Schwarzschild, A., and Vager, Z. (1967). *Phys. Rev. Lett.* **19**, 373.
Bezakova, E., Stuchbery, A. E., Bolotin, H. H., Seale, W. A., Kuyucak, S., and van Isacker, P. (1997). to be published.
Borchers, R. R, Herskind, B., Bronson, J. D., Grodzins, L., Kalish, R., and Murnick, D. E. (1968). *Phys. Rev. Lett.* **20**, 424.
Bozorth, R. M. (1951). 'Ferromagnetism' (Van Nostrand: New York).
de Raedt, J. A. G., Holthiuzen, A. J., Rutten, A. J., Sterrenburg, W. A., and van Middelkoop, G. (1980). *Hyp. Interact.* **7**, 455.
de Waard, H., Uggerhøj, E., and Miller, G. L. (1975). *J. Appl. Phys.* **46**, 2264.
Eberhardt, J. L., and Dybdal, K. (1980). *Hyp. Interact.* **7**, 387.
Garber, D. A., Behar, M., Grabowski, Z. W., and King, Wm. C. (1974). *Z. Phys.* **270**, 163.
Goldberg, M. B., Knauer, W., Kumbartzki, G. J., Speidel, K.- H., Adloff, J. C., and Gerber, J. (1978). *Hyp. Interact.* **4**, 262.
Kieser, R., Kaplan, N., and Turrell, B. G. (1974). *Phys. Rev.* B **9**, 2165.
Krane, K. S. (1983). *Hyp. Interact.* **15/16**, 1069.
Krane, K. S., and Steyert, W. A. (1974). *Phys. Rev.* C **9**, 2063.
Krane, K. S., Murdoch, B. T., and Steyert, W. A. (1973). *Phys. Rev. Lett.* **30**, 321.
Lindgren, B., Karlsson, E., and Jonsson, B. (1976). *Hyp. Interact.* **1**, 505.
Lindhard, J., and Winther, A. (1971). *Nucl. Phys.* A **166**, 413.
Muggli, J. (1973). *Phys. Stat. Sol. (b)* **57**, 257.
Piqué, A., Brennan, J. M., Darling, R., Tanczyn, R., Ballon, D., and Benczer-Koller, N. (1989). *Nucl. Instrum. Methods* A **279**, 579.
Raman, S., Malarkey, C. H., Milner, W. T., Nestor, C. W., Jr., and Stelson, P. H. (1987). *Atomic Data Nucl. Data Tables* **36**, 1.
Shu, N. K. B., Melnik, D., Brennan, J. M., Semmler, W., and Benczer-Koller, N. (1980). *Phys. Rev.* C **21**, 1828.
Sie, S. H., Fraser, I. A., Greenberg, J. S., Shaw, A. H., Stokstad, R. G., and Bromley, D. A. (1971). *In* 'Hyperfine Interactions in Excited Nuclei', Vol. 1 (Eds G. Goldring and R. Kalish), p. 129 (Gordon and Breach: New York).
Sioshansi, P., Garber, D. A., King, W. C., Scharenberg, R. P., Steffen, R. M. and Wheeler, R. M., (1972). *Phys. Lett.* B **39**, 343.
Skaali, B., Kalish, R., and Herskind, B. (1976). *Hyp. Interact.* **1**, 381.
Stewart, G. A., Barclay, J. A., Don, C. G., Lester, L. N., and Wilson, G. V. H. (1977). *J. Phys.* C **10**, 3651.
Stuchbery, A. E., Anderssen, S. S., Bolotin, H. H., Byrne, A. P., Dracoulis, G. D., Fabricius, B., and Kibédi, T. (1992). *Z. Phys.* A **342**, 373.
Stuchbery, A. E., Heseltine, T. H., Anderssen, S. S., Bolotin, H. H., Byrne, A. P., Fabricius, B., and Kibédi, T. (1994). *Hyp. Interact.* **88**, 97.
Stuchbery, A. E., Anderssen, S. S., and Bezakova, E. (1996*a*). *Hyp. Interact.* **97/98**, 479.

Stuchbery, A. E., Anderssen, S. S., Byrne, A. P., Davidson, P. M., Dracoulis, G. D., and Lane, G. J. (1996*b*). *Phys. Rev. Lett.* **76**, 2246.
van Walle, E., Vandeplassche, D., Wouters, J., Severijns, N., and Vanneste, L. (1986). *Phys. Rev.* B **34**, 2014.
Visser, D., Niesen, L., and de Waard, H. (1984). *J. Phys.* F **14**, 2419.
Ward, D., Häusser, O., Andrews, H. R., Taras, P., Skensved, P., Rud, N., and Broude, C. (1979). *Nucl. Phys.* A **330**, 225.

Manuscript received 18 August, accepted 14 October 1997